

Article

Simple and Facile Fabrication of Anion-Vacancy-Induced MoO_{3-x} Catalysts for Enhanced Hydrogen Evolution Activity

Seunghwan Jo ¹, Young-Woo Lee ², John Hong ^{3,*} and Jung Inn Sohn ^{1,*}

¹ Division of Physics and Semiconductor Science, Dongguk University-Seoul, Seoul 04620, Korea; imdl.joseunghwan@gmail.com

² Department of Energy Systems, Soonchunhyang University, Asan 31538, Korea; ywlee@sch.ac.kr

³ School of Materials Science and Engineering, Kookmin University, Seoul 02707, Korea

* Correspondence: johnhong@kookmin.ac.kr (J.H.); junginn.sohn@dongguk.edu (J.I.S.); Tel.: +82-910-4665 (J.H.); +82-(22)-2603190 (J.I.S.)

Received: 30 September 2020; Accepted: 12 October 2020; Published: 14 October 2020



Abstract: Advanced catalysts for clean hydrogen generation and storage offer an attractive possibility for developing a sustainable and ecofriendly future energy system. Transition metal oxides (TMO) are appealing candidates to be largely considered as electrode catalysts. However, for practical applications, there are still challenges—the intrinsic catalytic properties of TMOs should be further improved and TMOs should be synthesized by practical routes for cost-effective and scalable production of catalysts. Therefore, finding promising ways to fabricate highly active TMOs with outstanding electrochemical hydrogen evolution performance is required. Here, we present a direct and facile synthetic approach to successfully provide highly efficient MoO_{3-x} catalysts with electrochemically active oxygen vacancies through a one-step thermal activation process on a Mo metal mesh. Variations in the oxidation states of molybdenum oxides can significantly increase the active sites of the catalysts and improve the electrochemical activity, making these oxide compounds suitable for hydrogen evolution reaction (HER). Compared to the bare Mo mesh and fully oxidized Mo (MoO_3) electrodes, the fabricated MoO_{3-x} electrode exhibits better electrochemical performance in terms of overpotentials and Tafel slope, as well as the electrochemical 1000 cycling stability, confirming the improved HER performance of MoO_{3-x} . This provides new insight into the simple procedure suitable for the large-production supply.

Keywords: transition metal oxides; anion deficient molybdenum trioxide (MoO_{3-x}); oxygen vacancy; hydrogen evolution reaction

1. Introduction

The development of new materials for efficient energy generation is of paramount importance in order to meet ever-increasing energy demands and to provide environmentally friendly energy sources. It is expected that hydrogen gas and corresponding energy applications from water-splitting reactions should be capable of providing both high energy capacity and renewable (ecofriendly) resources [1–3]. Further research on catalytic electrode materials for an efficient hydrogen evolution reaction (HER) are needed to maximize its catalytic performance. Currently, earth abundant transition metal-based oxides (TMOs) have emerged as promising alternative electrocatalysts for noble metal replacement based on theories and experiments on their metal active sites, electrical structures, and surface properties. Those electrode materials have demonstrated their catalytic efficiency and high catalyst stability during HER regardless of electrolyte pH [4–6]. There are still a lot of challenges involved in using these materials as industrial electrode candidates due to their relatively low catalyst performance compared

to noble metals, e.g., platinum, and their synthesis methods, which still lack scalability. Enhancing the manufacturing scalability of TMOs and finding their simple fabrication process into high intrinsic catalytic performance are issues that need to be addressed.

To this end, numerous studies are being solicited by introducing and engineering anion defects into the crystal structure of TMOs [7–9]. It has been reported that anion deficiency in TMOs can provide favorable electrochemical kinetics as a result of the reduction of transition metal orbitals, which are regarded as the electrochemical active sites to promote gas evolution reactions [10–12]. However, it has been noted that, in hydrogen electrode applications, TMOs with anion vacancies cannot maintain their original structure during the adsorption of electrolyte ions while generating hydrogen gas. In other words, failure to accomplish the structural stability of TMO materials will cause a drastic decrease in electrochemical cyclability. Nevertheless, it has been demonstrated that certain structured and layered materials with vacancies can successfully exploit the favorable electrochemical kinetics during the adsorption and desorption of ions [13–15]. For example, molybdenum trioxide (MoO_3) is one of the promising TMO candidates with layered structures. Among many oxide materials, Molybdenum oxide (MoO_3) is an environmentally benign and low-cost chemical compound, which shows HER performance. In particular, its orthorhombic phase with the layered morphology are electrochemically stable due to its unique structure [16,17]. Its catalytic activity and electrochemical properties can be systematically managed through the formation of anion vacancy with rigid structural stability. Specifically, anion deficient MoO_3 (MoO_{3-x}) can maintain its original layered characteristics consisting of distorted MoO_6 octahedron sites that allow electrolyte ions to favorably intercalate and react with Mo sites [18,19]. Therefore, MoO_{3-x} can be successfully used as the electrode material in lithium-ion batteries and supercapacitors, as well as HER systems. However, synthesizing MoO_{3-x} electrodes in a productive method remains a challenge due to its multistep synthetic process [20,21]. Especially, to induce oxygen vacancies, further hydrogen treatment under high vacuum is required, which cannot be the mass-productive method by using highly explosive H_2 gas. Moreover, instead of using Mo precursors, direct synthesis on molybdenum substrate can be crucial to fabricate the electrode in a productive and scalable level. This is because the Mo sources originating from Mo substrates (meshes) and oxygen atoms can be reacted and converted into MoO_{3-x} electrode when the oxygen sources are limited compared to the Mo sources.

Herein, we synthesize the molybdenum oxide electrode materials with a controlled level of oxygen vacancies through a simple and facile thermal activation process for HER electrocatalysts, exhibiting the enhanced electrochemical performance in an alkaline media. Synthesizing catalytic materials directly on its metal substrate, such as the Mo mesh, can be beneficial for efficiently utilizing the corresponding transition metal compounds instead of using active material ink combined with carbon compounds. It has been previously reported that MoO_3 can be obtained through the oxidation of a transition metal during annealing at a high temperature in an air atmosphere without additional precursors. Following the annealing process, placing the as-synthesized MoO_3 under a reducing atmosphere condition, such as H_2 gas, induced MoO_{3-x} [22–24]. Here, we successfully and simply produce MoO_{3-x} electrodes with the one-step oxidation process under argon on the Mo mesh. The remarkable material and morphological properties of MoO_{3-x} ensure that the catalytic electrode exhibits a relatively low overpotential with a Tafel slope of 69 mV dec^{-1} compared to that of MoO_3 with a Tafel slope of 91 mV dec^{-1} . Along with its enhanced HER performance, the MoO_{3-x} electrodes show negligible performance degradation even with 1000 cycles of the linear sweep voltammetry (LSV) measurements. This confirms the electrochemical properties of MoO_{3-x} synthesized by our simple and facile one-step oxidation process are comparable to the reported MoO_3 electrodes.

2. Results

Promising electrocatalyst candidates with thermodynamically certain energy in water electrolysis should be recognized as ideal candidates with the favorable absorption of hydrogen ions and the desorption of H_2 gas in terms of free energy of hydrogen absorption ($\Delta G_H^\circ \approx 0$) [25]. In this

regard, among noble metals, Pt is used as a conventional reference catalyst for HER due to its calculated ΔG_H° close to zero, and it shows high electrical conductivity and outstanding electrochemical performance. Pt/C is an electrocatalyst composed of platinum supported on carbon materials, which can synergistically employ its large surface area and a large number of corresponding active sites. Therefore, the electrochemical activity, electrode conductivity, and large surface area of target materials are critical as an important indicator to access ΔG_H° and electrochemical performance in HER [6].

The MoO_3 electrodes with anion vacancy and nanostructured morphology were simply synthesized by the thermal activation process. Firstly, oxygen vacancies in MoO_3 can improve the electrical conductivity of the electrode, which is reported in many other articles [26]. Second, the nanostructured morphology of the electrode can provide the large surface area. Figure 1 represents MoO_{3-x} synthesized by controlling the temperature of the activation process without the addition of a conventional reducing gas source, such as hydrogen. A cleaned Mo mesh was introduced at the middle of the thermal annealing quartz tube for thermal treatment under an ambient flow rate of Ar at different temperatures for MoO_{3-x} and MoO_3 . The MoO_{3-x} electrode was fabricated at low temperature condition ($\sim 450^\circ\text{C}$), and the MoO_3 electrode was synthesized at high temperature condition ($\sim 600^\circ\text{C}$). Moreover, the enhanced HER performance is reported due to the increased surface area of MoO_{3-x} since its nanostructure can enhance the activity of TMOs in catalytic reactivity. Combining all catalytic features, the as-prepared MoO_{3-x} electrodes can utilize the aforementioned advantages to improve the catalytic activity.

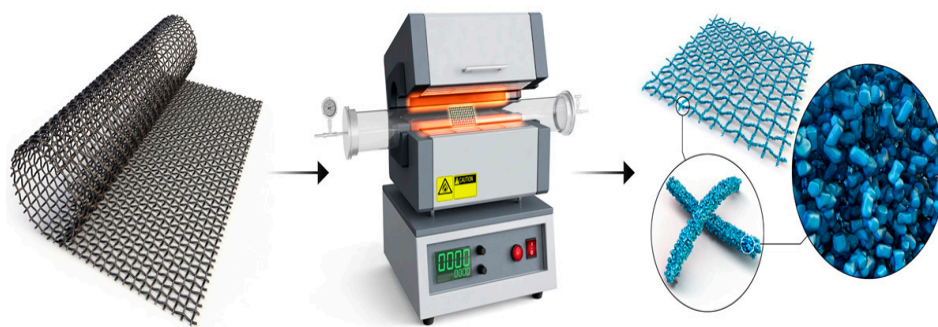


Figure 1. Schematic illustration of the MoO_{3-x} electrodes and their synthesis process.

To assess the morphological properties of MoO_3 and MoO_{3-x} , various scanning electron microscopy (SEM) analysis techniques were carried out. Figure 2b,c,e,f shows the SEM images of MoO_{3-x} and MoO_3 , respectively. As can be seen from low-magnification SEM images, the molybdenum trioxide materials were grown and uniformly distributed on the Mo mesh for both the samples. With the higher magnification, the MoO_{3-x} electrode shows the small nanosized grains with a diameter size of 200–400 nm. In contrast, the larger microsized grains were found in the MoO_3 electrode. Based on the SEM results, it can be confirmed that MoO_{3-x} , with a smaller particle size than MoO_3 , will provide the large specific surface area and a large number of the corresponding electrochemically active sites. Finally, Figure 2a,d represents the schematic illustration of both MoO_{3-x} and MoO_3 electrodes, respectively. We have used the lack of oxygen conditions to induce the oxygen vacancy in the MoO_{3-x} electrodes. After the low-temperature heat treatment, even though the temperature is high enough to overcome the activation energy of oxidization, there are not enough oxygen sources to react with the Mo substrate. Therefore, oxygen vacancies were generated. During the oxidation process, the adsorption of oxygen on the surface of metal is usually not a rate-limiting step. However, due to the lack of oxygen and the abundance of metal sources, it becomes a rate-limiting step, and the oxygen vacancies of MoO_3 occur [27].

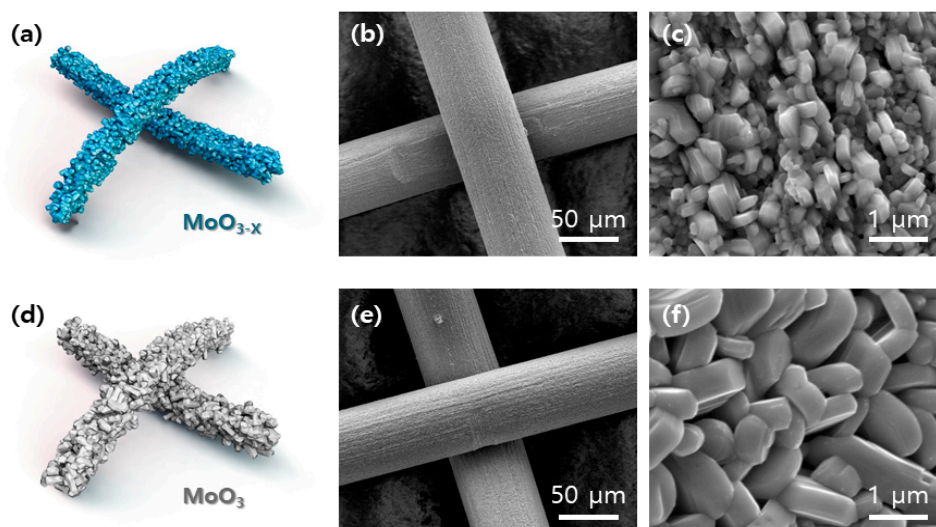


Figure 2. Schematic illustration of the as-prepared (a) MoO_{3-x} and (d) MoO_3 electrodes. Low-magnification scanning electron microscopy (SEM) images of (b) MoO_{3-x} and (e) MoO_3 . High-magnification SEM images of (c) MoO_{3-x} and (f) MoO_3 .

In Figure 3a, the color change of MoO_3 proves the presence of oxygen vacancies. The MoO_{3-x} electrode has a blue color on the surface of the Mo mesh, while the as-synthesized MoO_3 electrode possesses a bright gray and black color after the excess thermal activation process. Similar to the cases with other oxygen-deficient materials such as WO_{3-x} , it has been noted that the blue color of the TMO is induced from characteristic outer d-shell electron density (the delocalization of the electron density) [28–30]. In the MoO_{3-x} articles, the presence of oxygen vacancy has been signified through the color change [22]. The blue color of the as-prepared MoO_{3-x} electrode might be the indirect evidence to prove the presence of oxygen vacancy. To further understand the crystal phases and oxidation states, the MoO_3 and MoO_{3-x} electrodes were examined by Raman and X-ray photoelectron spectroscopy (XPS) as shown in Figure 3b–d. From the Raman spectroscopy in Figure 3b, three sharp peaks at 280 cm^{-1} , 663 cm^{-1} , and 818 cm^{-1} are identified and well assigned to the orthorhombic MoO_3 . Moreover, two relatively distinct peaks at 490 cm^{-1} and 890 cm^{-1} correspond to the stretching mode of MoO_{3-x} [10,31]. The surface electronic and oxidation states of the as-prepared samples were characterized by XPS. Figure 3c,d compares the high resolution XPS spectra of the Mo 3d of MoO_{3-x} and MoO_3 , respectively. The Mo^{6+} 3d doublet is clearly observed at about 235.9 eV ($\text{Mo}^{6+} 3d_{3/2}$) and at 232.7 eV ($\text{Mo}^{6+} 3d_{5/2}$) with a d spin-orbit splitting of 3.13 eV . Moreover, there are two additional doublets at 234.7 eV and 231.5 eV , indicating the oxidation states of Mo^{5+} , which cannot be found in the XPS spectra of MoO_3 , as shown in Figure 3d [14–16]. The various material characterization results based on the SEM, XPS, and Raman spectroscopy demonstrate that the existence of anion deficiency and nanostructured surface morphologies on the electrodes will be beneficial for the overall electrochemical activity. The oxygen vacancy and reduced oxidation states may improve the electrical conductivity of the electrode because of the increased carrier concentration. Moreover, the incorporation of oxygen vacancies can provide more surface active sites and enhance mass transport kinetics [14,21].

The electrocatalytic activity of the as-synthesized MoO_{3-x} and MoO_3 electrodes was examined in an alkaline aqueous solution (0.1 M KOH). In all experiments, the three-electrode system with Pt and Ag/AgCl was used as the counter electrode and reference electrode, respectively, while the Mo mesh with MoO_3 and MoO_{3-x} was used as the working electrode. In addition, the 20 wt% Pt/C was used as the reference electrocatalyst to objectively figure out the performance of the as-synthesized electrodes. Linear sweep voltammetry (LSV) was performed to measure the electrochemical performance of the electrocatalysts (Figure 4b–d), and to compare the effects of the anion deficiency of the as-synthesized MoO_{3-x} electrodes. Schematically, HER begins through the transfer of electrolyte ions, which are being

drawn by the applied potentials on working electrodes (Figure 4a). The polarization curves in Figure 4b show the generated electrons as the estimated current density (mA cm^{-2}), that is obtained by the adsorbed protons. The electrode reaches at a current density of 10 mA cm^{-2} at a potential of 187 mV for the MoO_{3-x} electrode, while the overpotential of MoO_3 at a current density of 10 mA cm^{-2} is at 261 mV. This overpotential value of MoO_{3-x} is closer to that of the Pt/C catalyst system (56 mV at a current density of 10 mA cm^{-2}) compared to MoO_3 , indicating the enhanced catalytic activity of MoO_{3-x} . The LSV curves also demonstrate that the significant effects of the existence of anion deficiency also result in the overpotential reduction at a current density of 50 mA cm^{-2} . The comparative Tafel plots and calculated Tafel slopes are derived from the polarization curves. The oxidation state of Mo is strongly related to how well Mo can carry out a series of the corresponding hydrogen reduction and adsorption processes (HER). The performance of the MoO_{3-x} electrodes is improved, but still follows the Heyrovsky mechanism [32,33]. In Figure 4c, the commercial Pt/C sample shows a Tafel slope of 57 mV dec^{-1} . The MoO_3 and MoO_{3-x} electrodes show Tafel slopes of 91 mV dec^{-1} and 69 mV dec^{-1} , respectively, indicating enhancement of HER activity using the MoO_{3-x} electrode. Specifically, the effects of anion deficiency have shown the decrease of the Tafel slope by 22 mV dec^{-1} . In addition to the activity and Tafel slope of the samples, cycling stability is another critical concern for TMO electrocatalysts with anion vacancies. The cycled LSV was conducted for the stability test of MoO_{3-x} and an HER performance test under the same conditions. The cycled LSV was performed from +0.2 V versus reversible hydrogen electrode (RHE) to -0.4 V versus RHE for 1000 cycles with a slight initial increase, but negligible performance deterioration (15 mV and 12 mV increase at current density of 10 mA cm^{-2} and 50 mA cm^{-2} , respectively) as shown in Figure 4d, confirming the high electrochemical and structural stability of MoO_{3-x} in HER.

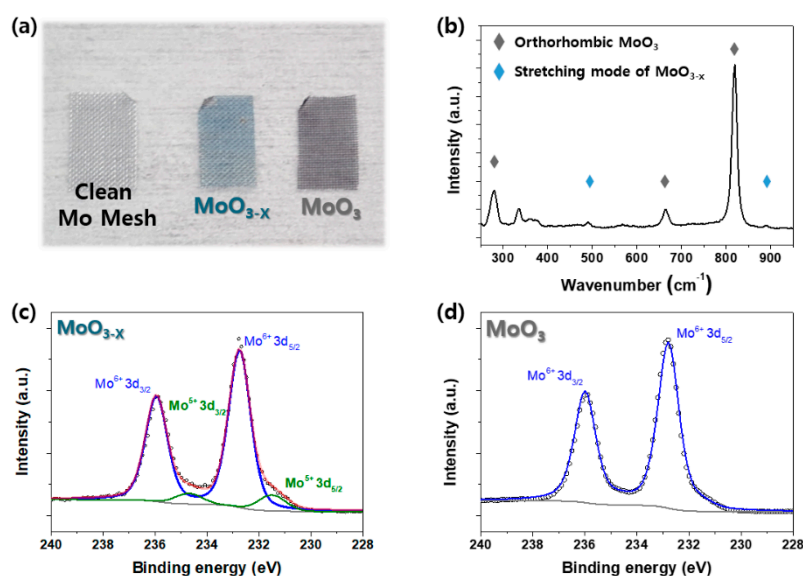


Figure 3. (a) Real photo images of the clean Mo mesh, MoO_{3-x} , and MoO_3 electrodes. (b) Raman spectra of MoO_{3-x} . Mo 3d X-ray photoelectron spectroscopy (XPS) spectra of (c) MoO_{3-x} and (d) MoO_3 .

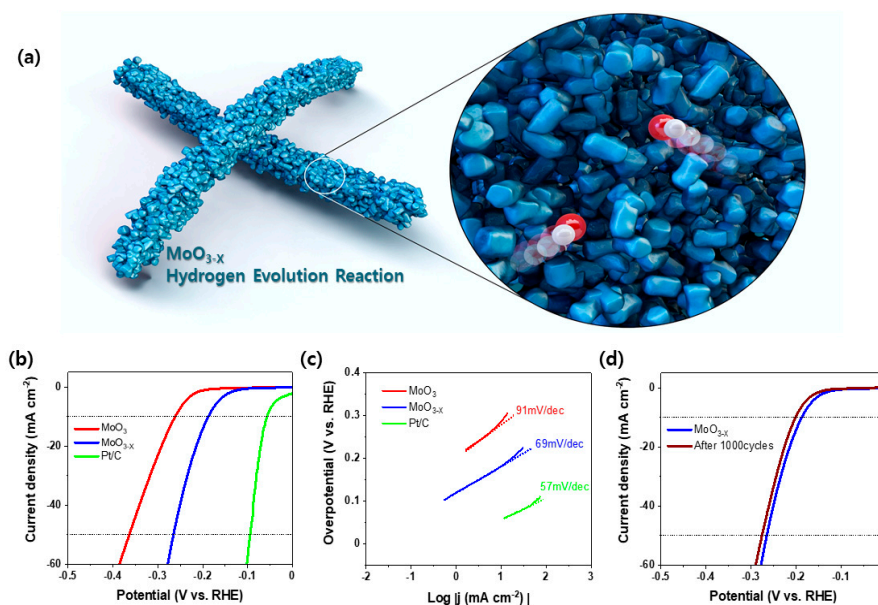


Figure 4. (a) Schematic illustration of the MoO_{3-x} electrode during hydrogen evolution reactions. (b) Polarization curves of the MoO₃, MoO_{3-x}, and Pt/C electrodes. (c) Tafel plots of the MoO₃, MoO_{3-x}, and Pt/C electrodes. (d) Stability test of the MoO_{3-x} electrode.

3. Materials and Methods

3.1. Preparations of Materials

The structured MoO_{3-x} electrodes were synthesized by the simple thermal oxidation process on the Mo mesh. First, the Mo mesh (Fisher Scientific, Hampton, NH, USA) was ultrasonically cleaned in ethanol, iso-propanol, and deionized water, and blown dry with nitrogen. The Mo mesh was introduced at the middle of the quartz tube, which was placed in the tube furnace. The temperature of the furnace was raised to the reaction temperature of 450–600 °C at a ramp rate of 5 °C/min under an ambient flow rate of Ar at 30 standard cubic centimeters per minute (sccm), and the sample was thermally oxidized for 2 h in an argon atmosphere.

3.2. Material Characterization

The morphologies of the as-prepared electrodes were investigated by scanning electron microscopy (SEM) using Hitachi S-4300 (Hitachi, Oxford, UK). Raman spectroscopy was conducted using Jobin Yvon LabRam Aramis Raman spectroscopy (Oxford, UK) with a 532 nm laser with a power of ~20 μW and a spot size of 1.09 μm² under ambient pressure and room temperature. X-ray photoelectron spectroscopy (XPS, Oxford, UK) was performed on a Thermo scientific K-Alpha instrument with an Al Kα X-ray source. The spectrometer was adjusted to align a binding energy of 284.5 eV for the C 1s line.

3.3. Electrochemical Measurements

HER catalytic activity tests were carried out in a standard three-electrode setup controlled by a Metrohm Autolab (Metrohm, Oxford, UK, 2019). A working electrode (Mo oxides with an Mo mesh), an Ag/AgCl (in 1 M KCl, aq) reference electrode, a graphite rod counter electrode, and a 0.1 M KOH solution as the electrolyte were used. The reference electrode was calibrated against and converted to a reversible hydrogen electrode (RHE).

4. Conclusions

The direct and facile synthesis method for the fabrication of the MoO_{3-x} electrode has been validated in this study. The MoO_{3-x} electrode was obtained directly through a thermal activation

process on the Mo mesh, which is used as the working electrode with high electrical conductivity and large surface area, as well as the Mo precursor-free synthesis. By applying the activation procedures without the additional Mo metal precursors, the MoO₃ and nonstoichiometric MoO_{3-x} electrodes with oxygen vacancies were fabricated on the surface of the Mo mesh. The MoO_{3-x} electrodes showed superior performance in HER. The MoO_{3-x} electrodes require a potential of 187 mV versus RHE to obtain a current density of 10 mA cm⁻², which is 74 mV less than the MoO₃ electrode and also represents the negligible electrocatalytic degradation during 1000 cycles of LSV. The verification of the effective one-step synthetic method by simply controlling the oxygen levels in TMOs could contribute to their practical applications in the hydrogen catalytic field.

Author Contributions: Conceptualization, S.J. and J.H.; methodology, S.J. and J.H.; validation, S.J., Y.-W.L., and J.H.; formal analysis, S.J. and J.H.; investigation, S.J. and J.H.; resources, S.J. and J.H.; data curation, S.J. and J.H.; writing—original draft preparation, S.J., J.H., and J.I.S.; writing—review and editing, S.J., Y.-W.L., J.H., and J.I.S.; visualization, Y.-W.L., J.H., and J.I.S.; supervision, J.H. and J.I.S.; project administration, J.H. and J.I.S.; funding acquisition, J.H. and J.I.S. All authors have read and agreed to the published version of the manuscript.

Funding: This research was funded by the National Research Foundation of Korea (NRF) grant funded by the Korean government (MSIT) (2019R1A2C1007883, 2019M1A2A2065616 and 2020R1F1A1068979).

Conflicts of Interest: The authors declare no conflict of interest.

References

1. Dresselhaus, M.S.; Thomas, I.L. Alternative energy technologies. *Nature* **2014**, *414*, 332–337. [[CrossRef](#)]
2. Schlapbach, L. Hydrogen-fuelled vehicles. *Nature* **2009**, *406*, 809–811. [[CrossRef](#)] [[PubMed](#)]
3. Turner, J.A. A realizable renewable energy future. *Science* **1999**, *285*, 687–689. [[CrossRef](#)] [[PubMed](#)]
4. Lu, Q.; Yu, Y.; Ma, Q.; Chen, B.; Zhang, H. 2D transition-metal-dichalcogenide-nanosheet-based composites for photocatalytic and electrocatalytic hydrogen evolution reactions. *Adv. Mater.* **2016**, *28*, 1917–1933. [[CrossRef](#)] [[PubMed](#)]
5. Zhu, Y.P.; Guo, C.; Zheng, Y.; Qiao, S.Z. Surface and interface engineering of noble-metal-free electrocatalysts for efficient energy conversion processes. *Acc. Chem. Res.* **2017**, *50*, 915–923. [[CrossRef](#)]
6. Zheng, Y.; Jiao, Y.; Jaroniec, M.; Qiao, S.Z. Advancing the electrochemistry of the hydrogen evolution reaction through combining experiment and theory. *Angew. Chem.* **2015**, *54*, 52–65. [[CrossRef](#)]
7. Xu, L.; Jiang, Q.; Xiao, Z.; Li, X.; Huo, J.; Wang, S.; Dai, L. Plasma-engraved Co₃O₄ nanosheets with oxygen vacancies and high surface area for the oxygen evolution reaction. *Angew. Chem.* **2016**, *55*, 5277–5281. [[CrossRef](#)]
8. Liu, R.; Wang, Y.; Liu, D.; Zou, Y.; Wang, S. Water-plasma-enabled exfoliation of ultrathin layered double hydroxide nanosheets with multivacancies for water oxidation. *Adv. Mater.* **2017**, *29*, 1701546. [[CrossRef](#)]
9. Kim, J.; Yin, X.; Tsao, K.-C.; Fang, S.; Yang, H. Ca₂Mn₂O₅ as oxygen-deficient perovskite electrocatalyst for oxygen evolution reaction. *J. Am. Chem. Soc.* **2014**, *136*, 14646–14649. [[CrossRef](#)]
10. Wu, M.; Ke, S.; Chen, W.; Zhang, S.; Zhu, M.; Zhang, Y.; Foo, M.L.; Tang, L. Optimization of the facet structure of cobalt oxide catalysts for enhanced hydrogen evolution reaction. *Catal. Sci. Technol.* **2020**, *10*, 1040–1047. [[CrossRef](#)]
11. Lovell, E.; Lu, X.; Zhang, Q.; Scott, J.; Amal, R. From passivation to activation—tunable nickel/nickel oxide for hydrogen evolution electrocatalysis. *Chem. Commun.* **2020**, *56*, 1709–1712. [[CrossRef](#)] [[PubMed](#)]
12. Nayak, A.K.; Verma, M.; Sohn, Y.; Deshpande, P.A.; Pradhan, D. Highly active tungsten oxide nanoplate electrocatalysts for the hydrogen evolution reaction in acidic and near neutral electrolytes. *ACS Omega* **2017**, *2*, 7039–7047. [[CrossRef](#)] [[PubMed](#)]
13. Liu, S.; Chen, C.; Zhang, Y.; Zheng, Q.; Zhang, S.; Mu, X.; Chen, C.; Ma, J.; Mu, S. Vacancy-coordinated hydrogen evolution reaction on MoO_{3-x} anchored atomically dispersed MoRu pairs. *J. Mater. Chem. A* **2019**, *7*, 14466–14472. [[CrossRef](#)]
14. Kim, H.; Cook, J.B.; Lin, H.; Ko, J.S.; Tolbert, S.H.; Ozolins, V.; Dunn, B. Oxygen vacancies enhance pseudocapacitive charge storage properties of MoO_{3-x}. *Nat. Mater.* **2017**, *16*, 454–460. [[CrossRef](#)] [[PubMed](#)]
15. Shen, S.; Zhang, X.; Cheng, X.; Xu, Y.-M.; Gao, S.; Zhao, H.; Zhou, X.; Huo, L.-H. Oxygen-vacancy-enriched porous α-MoO₃ nanosheets for trimethylamine sensing. *ACS Appl. Nano Mater.* **2019**, *2*, 8016–8026. [[CrossRef](#)]

16. Yu, M.; Shao, H.; Wang, G.; Yang, F.; Liang, C.; Rozier, P.; Wang, C.-Z.; Lu, X.; Simon, P.; Feng, X. Interlayer gap widened α -phase molybdenum trioxide as high-rate anodes for dual-ion-intercalation energy storage devices. *Nat. Commun.* **2020**, *11*, 1348. [CrossRef]
17. Brezesinski, T.; Wang, J.; Tolbert, S.H.; Dunn, B. Ordered mesoporous α -MoO₃ with iso-oriented nanocrystalline walls for thin-film pseudocapacitors. *Nat. Mater.* **2010**, *9*, 146–151. [CrossRef]
18. Yazdani, S.; Kashfi-Sadabad, R.; Huan, T.D.; Morales-Acosta, M.D.; Pettes, M.T. Polyelectrolyte-assisted oxygen vacancies: A new route to defect engineering in molybdenum oxide. *Langmuir* **2018**, *34*, 6296–6306. [CrossRef]
19. Shi, X.-R.; Wang, J.; Hermann, K. Theoretical cluster studies on the catalytic sulfidation of MoO₃. *J. Phys. Chem. C* **2010**, *114*, 6791–6801. [CrossRef]
20. Borgschulte, A.; Sambalova, O.; Delmelle, R.; Jenatsch, S.; Hany, R.; Nüesch, F. Hydrogen reduction of molybdenum oxide at room temperature. *Sci. Rep.* **2017**, *7*, 40761. [CrossRef]
21. Wu, Q.-L.; Zhao, S.-X.; Yu, L.; Zheng, X.-X.; Wang, Y.-F.; Yu, L.-Q.; Nan, C.-W.; Cao, G. Oxygen vacancy-enriched MoO_{3-x} nanobelts for asymmetric supercapacitors with excellent room/low temperature performance. *J. Mater. Chem. A* **2019**, *7*, 13205–13214. [CrossRef]
22. Luo, Z.; Miao, R.; Huan, T.D.; Mosa, I.M.; Poyraz, A.S.; Zhong, W.; Cloud, J.E.; Kriz, D.A.; Thanneeru, S.; He, J.; et al. Mesoporous MoO_{3-x} material as an efficient electrocatalyst for hydrogen evolution reactions. *Adv. Energy Mater.* **2016**, *6*, 1600528. [CrossRef]
23. Liu, J.; Zhu, D.; Zheng, Y.; Vasileff, A.; Qiao, S.Z. Self-supported earth-abundant nanoarrays as efficient and robust electrocatalysts for energy-related reactions. *ACS Catal.* **2018**, *8*, 6707–6732. [CrossRef]
24. Zhao, H.; Zhu, Y.-P.; Yuan, Z.-Y. Three-dimensional electrocatalysts for sustainable water splitting reactions. *Eur. J. Inorg. Chem.* **2016**, *2016*, 1916–1923. [CrossRef]
25. Zou, X.; Zhang, Y. Noble metal-free hydrogen evolution catalysts for water splitting. *Chem. Soc. Rev.* **2015**, *44*, 5148. [CrossRef]
26. Kashfi-Sadabad, R.; Yazdani, S.; Huan, T.D.; Cai, Z.; Pettes, M.T. Role of oxygen vacancy defects in the electrocatalytic activity of substoichiometric molybdenum oxide. *J. Phys. Chem. C* **2018**, *122*, 18212–18222. [CrossRef]
27. Oleksak, R.P.; Kapoor, M.; Perea, D.; Holcomb, G.R.; Doğan, Ö.N. The role of metal vacancies during high-temperature oxidation of alloys. *NPJ Mater. Degrad.* **2018**, *2*, 25. [CrossRef]
28. Yamashita, T.; Yokoyama, H. Molybdenum anode: A novel electrode for enhanced power generation in microbial fuel cells, identified via extensive screening of metal electrodes. *Biotechnol. Biofuels* **2018**, *11*, 39. [CrossRef]
29. Xu, Y.; Zheng, C.; Wang, S.; Hou, Y. 3D arrays of molybdenum sulphide nanosheets on Mo meshes: Efficient electrocatalysts for hydrogen evolution reaction. *Electrochim. Acta* **2015**, *174*, 653–659. [CrossRef]
30. Manthiram, K.; Alivisatos, A.P. Tunable localized surface plasmon resonances in tungsten oxide nanocrystals. *J. Am. Chem. Soc.* **2012**, *134*, 3995–3998. [CrossRef]
31. Dieterle, M.; Weinberg, G.; Mestl, G. Raman spectroscopy of molybdenum oxides. *Phys. Chem. Chem. Phys.* **2002**, *4*, 812–821. [CrossRef]
32. Li, Y.; Wang, H.; Xie, L.; Liang, Y.; Hong, G.; Dai, H. MoS₂ Nanoparticles grown on graphene: An advanced catalyst for the hydrogen evolution reaction. *J. Am. Chem. Soc.* **2011**, *133*, 7296–7299. [CrossRef] [PubMed]
33. Datta, R.S.; Haque, F.; Mohiuddin, M.; Carey, B.J.; Syed, N.; Zavabeti, A.; Zhang, B.; Khan, H.; Berean, K.J.; Ou, J.Z.; et al. Highly active two dimensional α -MoO_{3-x} for the electrocatalytic hydrogen evolution reaction. *J. Mater. Chem. A* **2017**, *5*, 24223–24231. [CrossRef]

Publisher's Note: MDPI stays neutral with regard to jurisdictional claims in published maps and institutional affiliations.



© 2020 by the authors. Licensee MDPI, Basel, Switzerland. This article is an open access article distributed under the terms and conditions of the Creative Commons Attribution (CC BY) license (<http://creativecommons.org/licenses/by/4.0/>).